How will global carbon cycle respond to negative emissions?

So-Won Park[1†], Kyung Min Noh[1†], Soon-Il An[2], Jonghun Kam[1,3], Eun-Young Kwon[4], Seung-Ki Min[1,3], Rokjin Park[5], Seok-Woo Son[5], Sang-Wook Yeh[6], and Jong-Seong Kug[1,3*]

[1]Division of Environmental Science and Engineering, Pohang University of Science and Technology (POSTECH), Pohang, South Korea
[2]Department of Atmospheric Sciences/Irreversible Climate Change Research Center, Yonsei University, Seoul, South Korea
[3]Institute for Convergence Research and Education in Advanced Technology, Yonsei University, Seoul, South Korea
[4]Center for Climate Physics, Institute for Basic Science, Busan, South Korea, 2Pusan National University, Busan, South Korea
[5]School of Earth and Environmental Sciences, Seoul National University, Seoul, South Korea
[6]Department of Marine Science and Convergent Technology, Hanyang University, Ansan, South Korea

*Corresponding authors: Jong-Seong Kug (jskug1@gmail.com)

†: These authors contributed equally to this work.

Abstract

In most emissions scenarios consistent with the temperature targets of the Paris Agreement, carbon dioxide removal (CDR) would be required to achieve net negative emissions. The efficiency of CDR depends on the behavior of the natural carbon reservoirs, land and ocean, that regulate atmospheric CO_2 concentrations, but their change in response to negative emissions is highly uncertain. Here, we investigate the response of the terrestrial and oceanic carbon cycle to negative emissions based on an idealized emission-driven simulation using a state-of-the-art Earth system model. The terrestrial and oceanic carbon sinks become carbon sources ~30 years after the onset of negative emissions. Thereafter, although the atmospheric CO_2 concentration returns to its initial level, the terrestrial ecosystem and the ocean continue to release carbon. The ocean recovers as a carbon sink within a few decades, while the terrestrial ecosystem remains a carbon source until the end of the simulation. The prolonged carbon emissions from the land are due to the delayed response of respiration to the earlier increase in terrestrial carbon uptake. As a result, the total carbon stock on land gradually decreases but still remains higher than its initial state. The ocean carbon inventory shows an irreversible change within a few centuries due to the accumulation of anthropogenic CO_2 in the deep ocean, which would take more than centuries to be removed naturally.

Plain Language Summary

Over the past few centuries, large amounts of anthropogenic CO_2 have been emitted into the atmosphere. The CO_2 concentration has now exceeded 400 ppm, which is the result of a balance between anthropogenic emissions and uptake by land and oceans. This increase in CO_2 concentration has led to various climate crises and, as a result, we need to remove CO_2 from the atmosphere and return it to the present climate levels using technologies such as carbon capture and storage (CCS). We have studied the response of the global carbon cycle to negative emissions using the state-of-the-art Earth System Model. Land and oceans, which normally absorb the anthropogenic CO_2 emitted, switch to an outgassing role after a few decades of negative emissions. Once the CO_2 concentration recovers to current climate levels, land and oceans respond differently due to their distinct processes involved in the carbon cycle. Land will continue to release CO_2 to the atmosphere because CO_2 emissions by soil respiration and fire exceed the net primary production over a prolonged period. On the other hand, the role of the oceans shifts from CO_2 outgassing to CO2 uptake within a few decades, contributing to the stabilization of atmospheric CO_2 at 430 ppm, about 50 ppm above the initial level. The ocean's carbon inventory is undergoing irreversible changes because the absorbed anthropogenic CO_2 is being transported to the deep ocean, which would take millennia to return to the surface. Therefore, the ocean needs more than several centuries to remove the anthropogenic carbon footprint in the interior of the ocean.

1. Introduction

Anthropogenic carbon dioxide (CO_2) emissions have been causing global warming since the pre-industrial era, which will persist and lead to further changes in the climate system, with adverse impacts on environment and lives (Carleton & Hsiang, 2016; Collins, 2013; IPCC, 2018; Matthews et al., 2009). To reduce climate change-induced risks, most countries adopted the Paris Agreement, whose the central objective is to pursue efforts to limit global warming to well below 2 °C, and preferably to 1.5 °C, compared to pre-industrial levels (UNFCCC, 2015). In most analyzed pathways consistent with these climate targets, anthropogenic CO_2 emissions should reach net zero and then net negative, and in this process, the use of carbon dioxide removal (CDR) should be necessary (Gasser et al., 2018; Rogelj et al., 2018). However, the effectiveness of CDR is uncertain due to a poor understanding of the future behavior of the global carbon cycle under net negative emissions (IPCC, 2018; Keller et al., 2018; Matthews et al., 2021; Schwinger et al., 2022a).

Land and ocean, major natural carbon (C) reservoirs that exchange CO_2 with the atmosphere, currently absorb almost half of the anthropogenic CO_2 emissions and are key factors in regulating atmospheric CO_2 concentrations (Friedlingstein et al., 2022). However, the rate of CO_2 uptake by land and ocean is sensitive to the changes in climate and atmospheric CO_2 concentrations (Arora et al., 2020; Heimann & Reichstein, 2008), and this rate may change or even may become a C source under negative emissions (Koven et al., 2023; Schwinger et al., 2022a). That is, the efficiency of CDR deployment depends on the behavior of natural C reservoirs under mitigation pathways—whether land and ocean will absorb or emit CO_2, and how much.

To date, we have indirectly assessed the CO_2 fluxes from land and ocean under negative emissions mainly using idealized CO_2 ramp-up and ramp-down experiments, such as climate and carbon cycle reversibility experiment (CDR-reversibility) and SSP5-3.4-overshoot scenario (Boucher et al., 2012; Chimuka et al., 2022; Keller et al., 2018; Koven et al., 2022; Melnikova et al., 2021; O'Neill et al., 2016; Park & Kug, 2022; Zickfeld et al., 2016; Ziehn et al., 2020). These studies have consistently shown that natural C sinks are enhanced during the CO_2 ramp-up period. However, during the CO_2 ramp-down period, they turn into C sources with a time lag of decades, demonstrating the existence of hysteresis in the global carbon cycle with respect to CO_2 concentrations.

However, because previous studies are mostly based on the concentration-driven simulations, it is still unclear how the hysteresis of global carbon cycles is directly linked with negative emissions. While CO_2 emissions can be inferred in these idealized concentration-driven experiments, the abrupt and large emissions reduction is required for the instantaneous change from positive to negative emissions, which creates a highly discontinuous and unrealistic emissions pathway (Boucher et al., 2012; Koven et al., 2023; Schwinger et al., 2022a). Furthermore, concentration-driven simulations cannot fully reflect the interactions between the climate system and the carbon cycle since atmospheric CO_2 concentrations do not respond to terrestrial and oceanic CO_2 fluxes (Hajima et al., 2014; IPCC, 2019; Jones et al., 2013). Therefore, an emission-driven simulation with more plausible assumptions using a state-of-the-art Earth system model is needed.

We thus designed an idealized CO_2 emissions pathway towards net negative emissions, assuming the gradual reduction of emissions through the continuous development of CDR technology, to avoid the unrealistic emissions pathway with sharp

discontinuity. Starting from the year 2000, anthropogenic emissions are increased linearly for 50 years based on the SSP5-8.5 scenario and then gradually reduced at the same rate for 147 years until the atmospheric CO_2 concentration returns to its initial value, allowing net zero and subsequent negative emissions. Thereafter, emissions are kept at net-zero until the year 2400 (Figure 1a, see Methods for details). This emission-driven experiment was conducted using the Community Earth System Model, version 2 (CESM2) (Danabasoglu et al., 2020).

The main goal of this study is to improve our understanding of the global carbon cycle's response to negative emissions. Specifically, we address the following questions: (1) How does the global carbon cycle respond under this emission pathway and regulate atmospheric CO_2 concentrations? (2) What are the major processes or driving mechanisms responsible for the changes in terrestrial and oceanic CO_2 fluxes? (3) How does the global carbon cycle interact with the climate system?

2. Methods

2.1. Model Configuration

CESM2 was used to perform an idealized CO_2 emission-driven simulation. This model consists of physical components, such as atmosphere, ocean, land, and cryosphere, which are fully coupled to the land and ocean carbon cycles (Danabasoglu et al., 2020). The atmosphere model is the Community Atmosphere Model version 6 (CAM6), which has a horizontal resolution with 1.25° in longitude and 0.9° in latitude, and 32 vertical layers. The ocean and sea ice models are the Parallel Ocean Program version 2 (POP2) (Danabasoglu et al., 2020; Smith et al., 2010) and the Community Ice CodE version 5

(CICE5) (Bailey et al., 2020). The ocean model has a uniform horizontal resolution of 1.125° in the zonal direction, and varying resolution in the meridional direction, with the finest resolution at the Equator (0.27°). It contains 60 vertical layers, with 20 layers concentrated in the upper ocean (up to ~200m).

The Community Land Model Version 5 (CLM5) (Lawrence et al., 2019), which represents the carbon and hydrological cycles in the land in CESM2, has achieved significant advances through implementation of new and updated processes and parameterizations. Key improvements include a better representation of cumulative CO_2 uptake and the seasonal cycle of net ecosystem production (Bonan et al., 2019; Collier et al., 2018; Lawrence et al., 2019). The CLM5 also implements a prognostic fire model and an explicit representation of agricultural management (Li et al., 2013; Li & Lawrence, 2017; Lombardozzi et al., 2020). We note that CLM5 does not include dynamic vegetation biogeography, and vegetation distributions are prescribed and held at the present-day condition (year 2000) (Oleson et al. 2013). The ocean carbon cycles in CESM2 are represented by the Marine Biogeochemistry Library (MARBL) (Long et al., 2021). This module includes fully prognostic carbonate chemistry, nutrient cycles, phytoplankton functional groups, and zooplankton. The biogeochemical variables interact with other spheres: atmospheric deposition of iron and riverine fluxes including nutrients, carbon, and alkalinity.

2.2. Experimental Design

We designed and performed an idealized negative emissions simulation to avoid discontinuity and increase feasibility in CO_2 emission pathway (Figure 1a). Specifically,

anthropogenic CO_2 emissions are increased linearly from 2000 to 2050, based on the SSP5-8.5 scenario (1.09 $GtCO_2$ increase per year), and then gradually reduced at the same rate until the global mean surface atmospheric CO_2 concentration recovers to its initial value (~383 ppm; year 2197); the reversal of net CO_2 emissions (from positive to negative) occurs in year 2124. Following the recovery of atmospheric CO_2 concentrations, net negative emissions cease and CO_2 emissions are maintained at zero from year 2197 to the end of the simulation (year 2400).

This simulation is an emission-driven run: Atmospheric CO_2 concentrations are determined not only by prescribed anthropogenic CO_2 emissions but also by terrestrial and oceanic CO_2 fluxes. All non-CO_2 conditions, such as land use and non-CO_2 greenhouse gas forcings, are kept at the present-day (2000) levels. To reduce the uncertainty, three ensemble members with slightly different initial conditions are considered.

3. Results

3.1. Global carbon cycle and climate system response to negative emissions

Land and ocean CO_2 fluxes show a similar temporal evolution for a given idealized emissions pathway, with similar magnitudes of the change (Figure 1a). As anthropogenic CO_2 emissions increase, the uptake of carbon by the land and oceans increases, reaching a maximum shortly after the peak of anthropogenic emissions. Subsequently, as anthropogenic emissions decrease, the amount of C sink gradually decreases, and land and ocean eventually become carbon sources with a lag of ~30 years after the onset of negative emissions. They reach the maximum carbon loss just before the onset of zero emissions ("restoring period") and then tend to recover to near zero CO_2 exchange rates with the

atmosphere, but with different recovery times: the oceanic CO_2 outgassing declines rapidly from its maximum (13. 5 $GtCO_2$ in 2196) to less than 1 $GtCO_2$ within 16 years, while terrestrial CO_2 fluxes show a slow recovery with greater interannual variability. It takes ~60 years for the terrestrial carbon loss to decrease from the maximum (16.9 $GtCO_2$ in 2194) to less than 1 $GtCO_2$. As a result, the cumulative carbon loss from land (786 $GtCO_2$) during the negative emissions and the restoring periods is much greater than that from the ocean (308 $GtCO_2$). This evolution of terrestrial and oceanic CO_2 fluxes is quite similar to that shown in the SSP5-3.4 overshoot scenarios and the CDR reversibility experiment (Koven et al., 2022, 2023; Melnikova et al., 2021; Park & Kug, 2022).

The change in atmospheric CO_2 concentrations is determined by the sum of prescribed anthropogenic emissions and terrestrial and oceanic CO_2 fluxes. The atmospheric CO_2 level peaks in the year 2107, when anthropogenic emissions are balanced with the combined C uptake by the ocean and land, and then begins to decline with decreasing CO_2 emissions, reaching a minimum in the year 2196. Thereafter, despite the cessation of the negative emissions (onset of net-zero emissions), atmospheric CO_2 concentrations rise again (~48 ppm) from year 2196 to 2270 due to continued C release from land and oceans and then gradually reach equilibrium. After about 1500 PgC of cumulative anthropogenic emissions from 2000 to 2123, about 800 PgC of artificial CO_2 removal would be required to restore the initial atmospheric CO_2 concentrations of the year 2000. However, the initial recovery of CO_2 concentrations is only temporary due to the ongoing C loss from land and ocean, so additional CO_2 removal will be required to fully restore CO_2 concentrations to the present climate levels.

Global mean near-surface air temperature (SAT) and precipitation (PRCP) change with CO_2 concentrations, but lag behind the radiative forcing due to the thermal inertia of the ocean after the CO_2 peak (Figure 1b) (Boucher et al., 2012; Cao et al., 2011; Hare & Meinshausen, 2006; Wigley, 2005; Wu et al., 2010): As CO_2 concentrations increase, both SAT and PRCP increase but show a delayed peak, after which they decrease slowly relative to their increase. This delay is particularly pronounced for precipitation, and further research is needed to investigate the underlying causes. During the restoring period, SAT and PRCP increase again due to the rebound in CO_2 concentrations, but these changes are much greater than those that occurred previously at the same level of CO_2 increase. These amplified responses can be partly attributed to the recovery of the Atlantic Meridional Overturning Circulation (AMOC): With global warming, the AMOC gradually weakens and the high latitude North Atlantic surface cools down, partially offsetting the global SAT increase. As the AMOC strengthens during the CO_2 reduction period, the AMOC transports more heat from the equator to the high latitudes, significantly increasing the global temperatures, especially in the Northern Hemisphere. This is consistent with the previous results shown in SSP5-3.4-overshoot scenarios and CDR-reversibility experiments (An et al., 2021; Koven et al., 2022; Kug et al., 2022; Schwinger et al., 2022a, b). This result implies that the level of global warming cannot return to its original state for at least hundreds of years, even if atmospheric CO_2 concentrations recover.

In summary, land and ocean, natural C sinks, contribute to the reduction of atmospheric CO_2 concentrations until decades after the onset of the net-negative emissions. However, they subsequently switch to C source, thereby reducing the effectiveness of CDR, which is in line with previous studies (Boucher et al., 2012; Chimuka et al., 2022; Park &

Kug, 2022; Zickfeld et al., 2016a). Although net-zero emissions are prescribed after the initial recovery of CO_2 concentrations, atmospheric CO_2 levels rise again due to continued C emissions from land and ocean. In addition, the recovery of the AMOC leads to global warming, which may affect the terrestrial and oceanic carbon cycle together with the rebound of atmospheric CO_2 during the restoring period. In the following sections, we examine the responses of the terrestrial and oceanic carbon cycles in more detail in order to better understand the changing role of C reservoirs under negative emissions.

3.2. Delayed terrestrial ecosystem carbon release in response to the negative emissions

The temporal evolution of land SAT and PRCP is somewhat different from the global mean response (Figures 2a and 1b). The change in land temperature is almost reversible during the changing CO_2 period, and strong re-warming occurs during the restoring period. There is no lagged response in land precipitation, which rather decreases faster than the rate of its increase. Subsequently, an overshoot of PRCP occurs at the end of changing CO_2, after which the PRCP increases again, above the level at the peak of CO_2 concentrations. Changes in the climate system as well as in CO_2 concentrations affect the terrestrial ecosystem processes, thereby regulating terrestrial C fluxes. Changes in net C uptake by vegetation, i.e., net primary production (NPP), are mainly driven by the CO_2 fertilization effect -an increased rate of photosynthesis with increasing CO_2 concentrations- and show a reversible response to CO_2 concentrations (Figure 2b) (Ainsworth & Long, 2005; Chimuka et al., 2022; Drake et al., 1997; Park & Kug, 2022). During the restoring period, NPP increases due to the rebound of CO_2, but this change is about 3 PgC/yr greater

246 than the previous response for the same CO_2 concentration change, due to the warmer and
247 wetter climate conditions.

248 This photosynthetic C gain is allocated to vegetation C pools (e.g. leaf, stem, and
249 root), and part of the biomass of each plant part enters the litter pool at different turnover
250 rates: e.g., fastest in leaves (Oleson et al., 2013). Fresh litter is gradually decomposed into
251 more recalcitrant forms (soil organic matter). Decomposition proceeds in multiple stages,
252 with rapid initial loss of labile compounds followed by slower loss of recalcitrant materials
253 (Bonan, 2019). To represent these different rates of decomposition of litter and soil C,
254 which depend on the chemical properties, and the different litterfall rates for each plant
255 part, multiple C pools system is introduced in the model. Each C pool (vegetation, litter,
256 and soil) exhibits the intrinsic lagged response to increasing C inputs (Figure 2c). In
257 addition, as C flows from plant to litter and then to soil, the peak of litter C lags behind
258 vegetation C, and the soil C pool lags even further. The soil C pool exhibits a significantly
259 delayed response and the slowest decline compared to the other C pools due to its slowest
260 decay rate.

261 The parts of C absorbed by the terrestrial ecosystem are released to the atmosphere
262 by microbial respiration or by wildfires. Fire C emissions show little change throughout
263 the simulation period, possibly due to underestimated sensitivity in the present model,
264 while heterotrophic respiration (HR) changes in amplitude similar to NPP but shows a
265 delayed response to CO_2 concentrations (Figure 2b). HR increases with increasing NPP,
266 peaks at the onset of negative emissions, and then begins to decrease slowly relative to its
267 increase. During the restoring period, HR approaches equilibrium and remains higher than
268 that in the positive emission phase at the same CO_2 concentrations.

This delayed response of HR can be caused by either or both lag in the climate system and the dead C pool (composed of litter and soil C), because the HR is primarily regulated by the climate system and the size of the litter-soil C pool. Microbial decomposition is enhanced by warmer and wetter conditions (Bond-Lamberty & Thomson, 2010; Orchard & Cook, 1983; Schlesinger & Andrews, 2000) and increased C input to the dead C pool, referred to as a priming effect (Bastida et al., 2019; Koven et al., 2015). To elucidate the mechanism of the delayed change in HR, we reconstructed the temporal evolution of HR from a multiple linear regression based on climate factors (SAT and PRCP) and factors associated with the terrestrial C cycle (NPP, litter, and soil C) (Figure S1). In the model, as both litter and soil C are represented by partitioning into multiple pools with different decay rates and the fastest litter pool exists, HR increases as fast as the rate of increase in NPP, while the dead C pool responds more slowly (Koven et al., 2015; Thompson et al., 1996). Therefore, NPP, litter C, and soil C are considered separately as key factors for the priming mechanism, taking their different decay rates into account.

It is shown that the warmer and wetter climate condition caused by increasing radiative forcing has only a small contribution to the HR change and this effect is reversible for CO_2 concentrations (Figure S1a). The main driver of HR change and its lag is the priming effect due to CO_2 fertilization: the delayed response of HR during negative and zero emissions is mainly due to the delayed increase of the litter-soil C pool and its slow decay rate (Figure S1b). This effect gradually diminishes over time. However, during the restoring period, HR increases slightly and remains high due to increased NPP and warmer and wetter conditions. In summary, the delayed response of HR to changes in atmospheric CO_2 is a remnant of the previous CO_2 increase, which is left by an inherent lag in terrestrial

292 ecosystem processes, resulting in continuous terrestrial C loss for at least centuries after
293 the CO_2 peak.

294 Consequently, the net atmosphere-land C flux, net biome production (NBP;
295 determined by the imbalance between NPP, HR, and fire C loss), is positive until decades
296 after the onset of negative emissions, demonstrating the well-known role of land as a C
297 sink (Friedlingstein et al., 2022). However, it becomes negative from the year 2153, when
298 the sum of HR and fire C loss exceeds NPP, which remains until the end of the simulation.
299 In conclusion, the terrestrial C loss lagging behind the onset of negative emissions is caused
300 by the intrinsic lag of terrestrial ecosystem processes to the previous increase in CO_2
301 concentrations. This persists until the end of the simulation, resulting in a rebound of CO_2
302 concentrations during the restoring period.

303

304 ***3.3. Latitudinal differences in response of terrestrial carbon cycle to negative emissions***

305 The response of the climate system and the terrestrial carbon cycle to negative
306 emissions varies by latitude (Figures 3a and 3b). Land SAT lags behind the radiative
307 forcing at all latitudes, consistent with the global mean (Figure 1b), except in the mid-high
308 Northern Hemisphere (NH). In this region, the increase in SAT is maximum at the CO_2
309 peak without delay, followed by a gradual cooling due to the decrease in the CO_2
310 concentrations and the weakening of the AMOC. As a result, the SAT anomaly reaches its
311 minimum at the lowest CO_2 level, followed by a significant warming comparable to its
312 peak with the recovery of the AMOC during the restoring period. The change in the land
313 PRCP in the northern mid-high latitudes follows that of the SAT. However, precipitation
314 in the equatorial region increases and NH off-equatorial precipitation decreases, throughout

315 the period of simulation. This might be associated with a narrowing of the intertropical
316 convergence zone and its southward shift (Kug et al., 2022).

317 In addition to the longer residence time of litter-soil C at high latitudes due to
318 slower decay rates in cold environments (Bird et al., 1996; Bloom et al., 2016; Wang et al.,
319 2018), these latitudinal differences in climate change cause a latitudinal dependence of the
320 terrestrial C cycle response to negative emissions. The change in terrestrial C fluxes is
321 concentrated in the tropics (10° S to 5° N) and mid-high latitudes (50° to 65° N), where
322 forest density is highest. The temporal evolution of NBP is similar at all latitudes, but the
323 transition from C sink to source is slower at higher latitudes (Figure 3b). In addition,
324 terrestrial C loss is weaker than C uptake at high latitudes, in contrast to the tropics where
325 the amplitudes of C uptake and loss are similar. That is, the total terrestrial C stock shows
326 a delayed response to CO_2, which is greater at high latitudes (Boucher et al., 2012; Park &
327 Kug, 2022; Ziehn et al., 2020).

328 To understand the regional differences in the lag times of the terrestrial C cycle,
329 we examined the temporal evolution of NPP and HR in the tropics and mid-high latitudes
330 (Figures 3c and 3d). In both regions, the NPP is reversible for the CO_2 concentrations prior
331 to the restoring period, while the HR lags behind the increase in NPP and decreases slowly.
332 Particularly at mid-high latitudes, HR remains high with little decrease and rather slightly
333 increases during the restoring period. This is due to the largest lag in the soil C pool at high
334 latitudes, with the slowest decay rates (Figure S2), and also due to the warmer and wetter
335 conditions associated with the re-strengthening of AMOC. In addition, this climatic
336 condition, together with the rebound of CO_2, significantly increases the NPP in this region,
337 where cold environments limit vegetation growth (Xu et al., 2013; Zhu et al., 2016). During

the restoring period, although the increased NPP partially contributes to the increase in HR, the increased NPP exceeds the increase in HR. As a result, NBP returns to slightly positive in high latitudes from the midpoint of the restoring period, which contributes to the maintenance of the terrestrial C stocks. On the other hand, in the tropics, NPP increases slightly but HR still remains high due to the delayed litter-soil C response. Consequently, the tropical land emits C during most of the restoring period, gradually reducing the total terrestrial C stock.

3.4. Ocean carbon release in response to the negative emissions

The ocean carbonate systems possess the ability to mitigate the escalating anthropogenic CO_2 emissions (Devries, 2022; Gruber et al., 2023), resulting in an increased ocean carbon inventory via air-sea CO_2 flux. The global ocean uptake of CO_2 has a strong linear dependence on the CO_2 growth rate (Melnikova et al., 2021), leading to a surge in the uptake of CO_2 that peaks three years after CO2 emissions peak (~4 PgC/yr, year 2053) (Figure 4a). Following the peak, the oceanic uptake subsequently declines as the growth rate of atmospheric CO_2 reduces. Under the negative CO2 emissions, the oceanic uptake continues to decrease until 2154, after which the ocean begins to release CO2 to the atmosphere, changing its status from a carbon sink to a carbon source. In 2196, atmospheric CO_2 concentration becomes identical to the present-day levels (year 2000). Nevertheless, oceanic surface DIC and pCO_2 levels are higher than those of 2000, leading to the outgassing CO_2 at a rate of about 4 PgC/yr, which is similar in magnitude to the peak CO_2 uptake in 2050 (Chimuka et al., 2022; Schwinger & Tjiputra, 2018). The resulting accumulation of oceanic CO_2 uptake leads to the continuous increase and subsequent peak

of ocean anthropogenic carbon (C_{ant}) inventory at 380 PgC in 2153 with a time lag of ~30 years from the start of negative emissions. During the restoring period, the slight increase in the C_{ant} inventory is associated with weak uptake of CO_2.

Responses of the ocean carbon cycle exhibit latitude-dependent patterns as in the land carbon cycle (Figures 4b). The evolutions of anomalous CO_2 flux are similar across most latitudes with increasing anomalous uptake as CO_2 emission increases and decreasing uptake as CO_2 emission decreases (Figures S4a). During the negative emissions, CO_2 uptake anomalies are reversed to CO_2 outgassing anomalies in most of the latitudinal bands. However, the intensity of the anomalies and the timings of sign changes vary with latitude. In mid-latitudes (around 25-50N or 25-50S) where the ocean surface currently acts as strong carbon sinks (Landschützer et al., 2014; Takahashi et al., 2009), the CO_2 uptake anomalies tend to become outgassing from uptake faster than the global average. On the other hand, the periods of positive CO_2 anomalies persist longer in the tropical and Southern Ocean (south of 60S). These different timing of transition can be partly explained by the fact that the re-emergence times of subsurface water (equilibrated with higher atmospheric pCO_2) tend to be shorter in subtropical gyres than in the tropical and Southern Ocean (Schwinger and Tjiputra, 2018; Toyama et al., 2017). Under the negative emissions, the carbon releases in the tropical oceans and the Southern Ocean intensify and the outgassing areas expand meridionally. As a result, the Sothern Ocean becomes a carbon source, except for marginal oceans near the Antarctic continent. Although the CO_2 concentration recovers to the present climate level, the role of the Southern Ocean remains a strong outgassing zone (Figure S5a, 0.3PgC/yr), of which CO_2 uptake contributes to

383 decadal variability of ocean carbon sink in the present climate (DeVries et al., 2019;
384 Frölicher et al., 2015; Gruber et al., 2019).

385 After the cessation of the negative emission in 2196, the air-sea CO_2 flux reaches
386 almost zero within a short period of ~22 years (Figure 4a), a typical time scale of upper
387 ocean ventilation (Galbraith et al., 2015). Consequently, the ocean resumes its role as a
388 carbon sink, releasing carbon (~17 PgC) into the atmosphere since the implementation of
389 zero emission. During the first decades of the zero emission, the carbon releases from land
390 and ocean are no longer counterbalanced by CO_2 removal from the atmosphere, resulting
391 in a rebound of atmospheric CO_2. The oceanic pCO_2 also increases and the average oceanic
392 pCO_2 remains higher than the atmospheric pCO_2 over the first 25 years of the restoring
393 period. Thereafter, the atmospheric CO_2 level slightly surpasses the oceanic pCO_2 level.
394 Due to this different timescale of rebounds in oceanic and atmospheric pCO_2, the ocean
395 transitions from a source to sink despite an increase in pCO_2.

396 To comprehend the oceanic processes responsible for the changes in air-sea CO_2
397 fluxes during the restoring period, it is necessary to investigate changes in pCO_2 because
398 global ocean uptake of CO_2 is predominantly influenced by geochemical processes rather
399 than physical climate changes (Arora et al., 2020; Arora et al., 2013; Friedlingstein et al.,
400 2022). The modulation of pCO_2 is typically associated with thermal factor, which is
401 regulated by sea surface temperature (SST), and non-thermal factors including dissolved
402 inorganic carbon (DIC), alkalinity (ALK), and sea surface salinity (SSS) (Orr et al., 2022;
403 Takahashi et al., 1993). Therefore, to assess the contributions of these potential drivers, we
404 use a Taylor expansion to decompose variations in pCO_2 after neglecting second-order
405 terms and normalizing the salinity effect to DIC and ALK (Supporting Information).
406

$$\Delta pCO_2 = \frac{\partial pCO_2}{\partial SST} \cdot \Delta SST + \frac{\partial pCO_2}{\partial DIC}\left(\frac{S}{S_0}\right) \cdot \Delta sDIC + \frac{\partial pCO_2}{\partial ALK}\left(\frac{S}{S_0}\right) \cdot \Delta sALK + \frac{\partial pCO_2}{\partial FW} \cdot \Delta FW$$

with freshwater flux (FW), normalized DIC ($sDIC = DIC \cdot S_0/S$) and ALK ($sALK = ALK \cdot S_0/S$) with reference salinity S_0 (Keeling et al., 2004; Wetzel et al., 2005).

Based on this climate-CO_2 Taylor separation, we quantify the contributions of individual drivers during the period of ocean recovery from a carbon source to a sink (year 2196 to 2220). The linear decomposition adequately replicates the original changes in pCO_2. Our analysis reveals that individual factors contribute to an increase in pCO_2 of approximately 1.8ppm (SST), 0.9 ppm (FW), 16.2 ppm (DIC), and -2.5 ppm (ALK) (Figure 4c). These findings suggest that the recovery process is directly influenced by the interaction between atmospheric CO_2 and ocean chemistry, which contributes to the relatively fast recovery compared to land surface CO_2 flux.

Although atmospheric CO_2 concentration almost recovers to present climate levels with slight increases, the anthropogenic carbon remains sequestered in the deep ocean (Figure 4d), with a value approximately 300 PgC higher than the current levels. During the positive emission, C_{ant} is taken up by the sea surface and transported to the subsurface through a process called water mass formation and subduction. A major portion of the subducted C_{ant} spreads to the global ocean through deep ocean circulation and remains sequestered from the atmosphere over multi-century timescales. Notably, C_{ant} is predominantly stored in the Atlantic Ocean and Southern Ocean (Figure S3) due to relatively short timescales for upper ocean ventilation via North Atlantic Deep Water and Subantarctic Mode Water (Gruber et al., 2019; Khatiwala et al., 2009; Sabine et al., 2004). When the ocean transitions from a carbon sink to a carbon source, C_{ant} is mainly released from the tropical and Southern Ocean, where previously sequestered C_{ant} is converged in

the thermocline and subsequently upwelled to the surface, elevating surface DIC and pCO_2. At the same time, the accumulated C_{ant} at depth continues to spread through meridional overturning circulation. However, the four centuries-long simulation is not long enough for the deep C_{ant} to reach the northern Pacific Ocean (Figure S3b), where the column integrated C_{ant} at the end of the simulation is reduced relative to that of 2000 (Figure 4d). The fact that C_{ant} is still not removed from the deep ocean suggests that the ocean carbonate system experiences irreversible changes over the simulation period, and millennial timescale persistent negative emissions would be required for this anthropogenic evidence to be naturally removed from the ocean (Mathesius et al., 2015).

4. Summary and Discussions

In this study, we investigate the response of global carbon cycle in response to the negative emissions through an idealized emission-driven experiment. The terrestrial and oceanic systems act as natural sinks for anthropogenic carbon under positive emissions. However, in response to negative emissions, the role of these carbon systems changes from a sink to a source with a time lag of ~30 years. Following the zero emissions, the ocean rapidly returns its role as a carbon sink, while the land continues to release carbon into the atmosphere, providing an additional CO_2 increase of ~50 ppm compared to the present-day level. The CO_2 concentration then reaches quasi-equilibrium during the restoring period. The delayed response of respiration allows the continuous carbon release from the terrestrial system with latitudinal dependency, leading to a reduction in land carbon stock. In contrast, the accumulated anthropogenic carbon, transported to the deep ocean by ocean circulation, cannot be naturally removed from the ocean interior within centuries and it

would take several millennia to reach the present climate state only if deep waters return to the sea surface under a lower atmospheric CO_2 level than the oceanic pCO_2 (Mathesius et al., 2015). For this, the Southern Ocean would play an increasingly more important role in venting out deeply sequestered anthropogenic CO_2 to the atmosphere. Even if so, how the global marine ecosystems would respond to such long-term disturbance and whether these responses might be reversible are highly uncertain.

Both land and ocean act as a C sink for the first 30 years after the onset of the negative emissions, contributing almost equally to the decrease in CO_2 concentration, but afterwards, they switch to a C source, reducing the efficiency of CDR. These results from the CESM2 emission-driven experiments are consistent with previous studies based on concentration-driven experiments (Boucher et al., 2012; Chimuka et al., 2022; Koven et al., 2022; Park & Kug, 2022; Zickfeld et al., 2016b) but provide more direct information about the role of land and ocean C cycle under the emission pathway towards negative emissions, which can be considered in climate mitigation policies. It is noted that continuous natural C emissions during the restoring period can cause the rebound of CO_2 concentration (~50 ppm), implying that the initial recovery of CO_2 is temporary and additional negative emissions are necessary for a complete return to the pre-industrial CO_2 levels.

Furthermore, even if the CO_2 concentration returns to its initial state, the climate conditions could be irreversible for at least centuries due to the recovery of the AMOC, which would induce surface warming, especially in high latitudes, in agreement with previous studies (An et al., 2021; Schwinger et al., 2022b). This warming at high latitudes, together with the rebound of CO_2, would increase vegetation productivity (Zhu et al., 2016)

as well as C release in permafrost (Schuur et al., 2015), thereby increasing the uncertainty in terrestrial C fluxes. Therefore, further research is needed to understand the changes in the C balance in permafrost regions.

As only the CESM2 model is used in this study, further research is needed in a multi-model context. Previous studies have shown the significant differences in the direction, magnitude or hysteresis lag of terrestrial and oceanic CO_2 fluxes among Earth System Models (ESMs) in the CDR reversibility experiment, the SSP5-3.4 overshoot scenario and the Zero Emissions Commitment Model Intercomparison Project (Koven et al., 2022; MacDougall et al., 2020; Park & Kug, 2022). Therefore, even under the same emission pathways as in this study, the amount of natural C uptake during the increasing CO_2 period, the delayed C release from natural C reservoirs, and its timing may differ between ESMs, resulting in different final states of CO_2 concentrations and the climate system.

Although most ESMs simulate the weakening and re-strengthening of the AMOC in overshoot scenarios or CDR reversibility experiments, CESM2 shows a particularly strong decline and rebound of the AMOC compared to other ESMs (Koven et al., 2022; Schwinger et al., 2022a, b). This AMOC behavior leads to stronger cooling and warming at high latitudes, which can affect various terrestrial ecosystem processes in the northern high latitudes, including permafrost. That is, the different behavior of the AMOC between ESMs increases uncertainties in both the climate system and the terrestrial CO_2 fluxes under negative emissions. Therefore, it is important to estimate the uncertainty in the response of the global carbon cycle and the AMOC under negative emissions in a multi-model framework and to consider this in the mitigation strategy.

Data Availability Statement

The data used in this study will be available from a figshare website (https://doi.org/10.6084/m9.figshare.23266265.v1).

Acknowledgments

JSK was supported by the National Research Foundation of Korea (NRF) grant funded by the Korean government (NRF2022R1A3B1077622; NRF-2021M3I6A1086808) and by the National Supercomputing Center with supercomputing resources including technical support (KSC-2022-CHA-0008). SIA was supported by by the National Research Foundation of Korea (NRF) grant funded by the Korean government (NRF-2018R1A5A1024958)

Author Contribution

S.-W. Park and K. M. Noh compiled the data, conducted analyses, prepared the figures, and wrote the manuscript. J.-S. Kug designed the research and wrote the manuscript. All of the authors discussed the results and reviewed the manuscript.

Competing Interests

The authors declare no competing interest.

References

Ainsworth, E. A., & Long, S. P. (2005). What have we learned from 15 years of free-air CO_2 enrichment (FACE)? A meta-analytic review of the responses of photosynthesis, canopy properties and plant production to rising CO_2. *New Phytologist*, *165*(2), 351–372. https://doi.org/https://doi.org/10.1111/j.1469-8137.2004.01224.x

An, S. Il, Shin, J., Yeh, S. W., Son, S. W., Kug, J. S., Min, S. K., & Kim, H. J. (2021). Global cooling hiatus driven by an AMOC overshoot in a carbon dioxide removal scenario. *Earth's Future*, *9*(7), e2021EF002165. https://doi.org/10.1029/2021EF002165

Arora, V. K., Katavouta, A., Williams, R. G., Jones, C. D., Brovkin, V., Friedlingstein, P., et al. (2020). Carbon–concentration and carbon–climate feedbacks in CMIP6 models and their comparison to CMIP5 models. *Biogeosciences*, *17*(16), 4173–4222. https://doi.org/10.5194/bg-17-4173-2020

Arora, V. K., Boer, G. J., Friedlingstein, P., Eby, M., Jones, C. D., Christian, J. R., et al. (2013). Carbon–Concentration and Carbon–Climate Feedbacks in CMIP5 Earth System Models. *Journal of Climate*, *26*(15), 5289–5314. https://doi.org/10.1175/JCLI-D-12-00494.1

Bailey, D. A., Holland, M. M., DuVivier, A. K., Hunke, E. C., & Turner, A. K. (2020). Impact of a New Sea Ice Thermodynamic Formulation in the CESM2 Sea Ice Component. *Journal of Advances in Modeling Earth Systems*, *12*(11), 1–15. https://doi.org/10.1029/2020MS002154

Bastida, F., García, C., Fierer, N., Eldridge, D. J., Bowker, M. A., Abades, S., et al. (2019). Global ecological predictors of the soil priming effect. *Nature Communications*, *10*(1), 3481. https://doi.org/10.1038/s41467-019-11472-7

Bird, M. I., Chivas, A. R., & Head, J. (1996). A latitudinal gradient in carbon turnover times in forest soils. *Nature*, *381*(6578), 143–146. https://doi.org/10.1038/381143a0

Bloom, A. A., Exbrayat, J. F., Van Der Velde, I. R., Feng, L., & Williams, M. (2016). The decadal state of the terrestrial carbon cycle: Global retrievals of terrestrial carbon allocation,

pools, and residence times. *Proceedings of the National Academy of Sciences of the United States of America*, *113*(5), 1285–1290. https://doi.org/10.1073/pnas.1515160113

Bonan, G. B. (2019). *Climate Change and Terrestrial Ecosystem Modeling*. Cambridge: Cambridge University Press. https://doi.org/10.1017/9781107339217

Bonan, G. B., Lombardozzi, D. L., Wieder, W. R., Oleson, K. W., Lawrence, D. M., Hoffman, F. M., & Collier, N. (2019). Model Structure and Climate Data Uncertainty in Historical Simulations of the Terrestrial Carbon Cycle (1850–2014). *Global Biogeochemical Cycles*, *33*(10), 1310–1326. https://doi.org/10.1029/2019GB006175

Bond-Lamberty, B., & Thomson, A. (2010). Temperature-associated increases in the global soil respiration record. *Nature*, *464*(7288), 579–582. https://doi.org/10.1038/nature08930

Boucher, O., Halloran, P. R., Burke, E. J., Doutriaux-Boucher, M., Jones, C. D., Lowe, J., et al. (2012). Reversibility in an Earth System model in response to CO_2 concentration changes. *Environmental Research Letters*, *7*(2), 024013. https://doi.org/10.1088/1748-9326/7/2/024013

Cao, L., Bala, G., & Caldeira, K. (2011). Why is there a short-term increase in global precipitation in response to diminished CO_2 forcing? *Geophysical Research Letters*, *38*(6), L06703. https://doi.org/10.1029/2011GL046713

Carleton, T. A., & Hsiang, S. M. (2016). Social and economic impacts of climate. *Science*, *353*(6304), aad9837. https://doi.org/10.1126/science.aad9837

Chimuka, V. R., Nzotungicimpaye, C.-M., & Zickfeld, K. (2022). Quantifying land carbon cycle feedbacks under negative CO_2 emissions. at *Biogeosciences Discussions*, 1–22. https://doi.org/10.5194/bg-2022-168

Collier, N., Hoffman, F. M., Lawrence, D. M., Keppel-Aleks, G., Koven, C. D., Riley, W. J., et al. (2018). The International Land Model Benchmarking (ILAMB) System: Design, Theory, and Implementation. *Journal of Advances in Modeling Earth Systems*, *10*(11), 2731–2754. https://doi.org/10.1029/2018MS001354

572 Collins, M. (2013). Long-term climate change: Projections, commitments and irreversibility.
573 *Climate Change 2013 the Physical Science Basis: Working Group I Contribution to the*
574 *Fifth Assessment Report of the Intergovernmental Panel on Climate Change*, *9781107057*,
575 1029–1136. https://doi.org/10.1017/CBO9781107415324.024
576 Danabasoglu, G., Lamarque, J.-F., Bacmeister, J., Bailey, D. A., DuVivier, A. K., Edwards, J., et
577 al. (2020). The Community Earth System Model Version 2 (CESM2). *Journal of Advances*
578 *in Modeling Earth Systems*, *12*(2), e2019MS001916.
579 https://doi.org/https://doi.org/10.1029/2019MS001916
580 Devries, T. (2022). The Ocean Carbon Cycle. *Annual Review of Environment and Resources*, *47*,
581 317–341. https://doi.org/10.1146/annurev-environ-120920-111307
582 DeVries, T., Le Quéré, C., Andrews, O., Berthet, S., Hauck, J., Ilyina, T., et al. (2019). Decadal
583 trends in the ocean carbon sink. *Proceedings of the National Academy of Sciences of the*
584 *United States of America*, *116*(24), 11646–11651. https://doi.org/10.1073/pnas.1900371116
585 Drake, B. G., Gonzàlez-Meler, M. A., & Long, S. P. (1997). MORE EFFICIENT PLANTS: A
586 Consequence of Rising Atmospheric CO_2? *Annual Review of Plant Physiology and Plant*
587 *Molecular Biology*, *48*(1), 609–639. https://doi.org/10.1146/annurev.arplant.48.1.609
588 Friedlingstein, P, O'Sullivan, M., Jones, M. W., Andrew, R. M., Gregor, L., Hauck, J., et al.
589 (2022). Global Carbon Budget 2022. *Earth Syst. Sci. Data*, *14*(11), 4811–4900.
590 https://doi.org/10.5194/essd-14-4811-2022
591 Friedlingstein, Pierre, Sullivan, M. O., Jones, M. W., Andrew, R. M., Gregor, L., Hauck, J., et al.
592 (2022). Global Carbon Budget 2022, 4811–4900.
593 Frölicher, T. L., Sarmiento, J. L., Paynter, D. J., Dunne, J. P., Krasting, J. P., & Winton, M.
594 (2015). Dominance of the Southern Ocean in anthropogenic carbon and heat uptake in
595 CMIP5 models. *Journal of Climate*, *28*(2), 862–886. https://doi.org/10.1175/JCLI-D-14-
596 00117.1

Gasser, T., Kechiar, M., Ciais, P., Burke, E. J., Kleinen, T., Zhu, D., et al. (2018). Path-dependent reductions in CO_2 emission budgets caused by permafrost carbon release. *Nature Geoscience*, *11*(11), 830–835. https://doi.org/10.1038/s41561-018-0227-0

Gruber, N., Clement, D., Carter, B. R., Feely, R. A., van Heuven, S., Hoppema, M., et al. (2019). The oceanic sink for anthropogenic CO_2 from 1994 to 2007. *Science*, *363*(6432), 1193–1199. https://doi.org/10.1126/science.aau5153

Gruber, N., Bakker, D. C. E., DeVries, T., Gregor, L., Hauck, J., Landschützer, P., et al. (2023). Trends and variability in the ocean carbon sink. *Nature Reviews Earth and Environment, 4,* 119–134. https://doi.org/10.1038/s43017-022-00381-x

Hajima, T., Kawamiya, M., Watanabe, M., Kato, E., Tachiiri, K., Sugiyama, M., et al. (2014). Modeling in Earth system science up to and beyond IPCC AR5. *Progress in Earth and Planetary Science*, *1*(1), 29. https://doi.org/10.1186/s40645-014-0029-y

Hare, B., & Meinshausen, M. (2006). How Much Warming are We Committed to and How Much can be Avoided? *Climatic Change*, *75*, 111–149. https://doi.org/10.1007/s10584-005-9027-9

Heimann, M., & Reichstein, M. (2008). Terrestrial ecosystem carbon dynamics and climate feedbacks. *Nature*, *451*(7176), 289–292. https://doi.org/10.1038/nature06591

IPCC, 2019: Summary for Policymakers. In: *Climate Change and Land: an IPCC special report on climate change, desertification, land degradation, sustainable land management, food security, and greenhouse gas fluxes in terrestrial ecosystems* [P.R. Shukla, J. Skea, E. Calvo Buendia, V. Masson-Delmotte, H.- O. Pörtner, D. C. Roberts, P. Zhai, R. Slade, S. Connors, R. van Diemen, M. Ferrat, E. Haughey, S. Luz, S. Neogi, M. Pathak, J. Petzold, J. Portugal Pereira, P. Vyas, E. Huntley, K. Kissick, M. Belkacemi, J. Malley, (eds.)]. https://doi.org/10.1017/9781009157988.001

IPCC, 2018: Summary for Policymakers. In: *Global Warming of 1.5°C. An IPCC Special Report on the impacts of global warming of 1.5°C above pre-industrial levels and related global*

greenhouse gas emission pathways, in the context of strengthening the global response to the threat of climate change, sustainable development, and efforts to eradicate poverty [Masson-Delmotte, V., P. Zhai, H.-O. Pörtner, D. Roberts, J. Skea, P.R. Shukla, A. Pirani, W. Moufouma-Okia, C. Péan, R. Pidcock, S. Connors, J.B.R. Matthews, Y. Chen, X. Zhou, M.I. Gomis, E. Lonnoy, T. Maycock, M. Tignor, and T. Waterfield (eds.)]. Cambridge University Press, Cambridge, UK and New York, NY, USA, pp. 3-24. https://doi.org/10.1017/9781009157940.001.

Jones, C., Robertson, E., Arora, V., Friedlingstein, P., Shevliakova, E., Bopp, L., et al. (2013). Twenty-first-century compatible CO_2 emissions and airborne fraction simulated by CMIP5 Earth system models under four representative concentration pathways. *Journal of Climate*, *26*(13), 4398–4413. https://doi.org/10.1175/JCLI-D-12-00554.1

Keeling, C. D., Brix, H., & Gruber, N. (2004). Seasonal and long-term dynamics of the upper ocean carbon cycle at Station ALOHA near Hawaii. *Geoscientific Model Development Global Biogeochemical Cycles*, *18*, 1–26. https://doi.org/10.1029/2004GB002227

Keller, D. P., Lenton, A., Scott, V., Vaughan, N. E., Bauer, N., Ji, D., et al. (2018). The Carbon Dioxide Removal Model Intercomparison Project (CDRMIP): rationale and experimental protocol for CMIP6. *Geoscientific Model Development*, *11*(3), 1133–1160. https://doi.org/10.5194/gmd-11-1133-2018

Khatiwala, S., Primeau, F., & Hall, T. (2009). Reconstruction of the history of anthropogenic CO2 concentrations in the ocean. *Nature*, *462*(7271), 346–349. https://doi.org/10.1038/nature08526

Koven, C. D., Chambers, J. Q., Georgiou, K., Knox, R., Negron-Juarez, R., Riley, W. J., et al. (2015). Controls on terrestrial carbon feedbacks by productivity versus turnover in the CMIP5 Earth System Models. *Biogeosciences*, *12*(17), 5211–5228. https://doi.org/10.5194/bg-12-5211-2015

Koven, C. D., Arora, V. K., Cadule, P., Fisher, R. A., Jones, C. D., Lawrence, D. M., et al. (2022). Multi-century dynamics of the climate and carbon cycle under both high and net negative emissions scenarios. *Earth System Dynamics*, *13*(2), 885–909. https://doi.org/10.5194/esd-13-885-2022

Koven, C. D., Sanderson, B. M., & Swann, A. L. S. (2023). Much of zero emissions commitment occurs before reaching net zero emissions. *Environmental Research Letters*, *18*(1), 14017. https://doi.org/10.1088/1748-9326/acab1a

Kug, J. S., Oh, J. H., An, S. Il, Yeh, S. W., Min, S. K., Son, S. W., et al. (2022). Hysteresis of the intertropical convergence zone to CO_2 forcing. *Nature Climate Change*, *12*(1), 47–53. https://doi.org/10.1038/s41558-021-01211-6

Landschützer, P., Gruber, N., Bakker, D. C. E., & Schuster, U. (2014). Recent variability of the global ocean carbon sink. *Global Biogeochemical Cycles*, *28*(9), 927–949. https://doi.org/https://doi.org/10.1002/2014GB004853

Lawrence, D. M., Fisher, R. A., Koven, C. D., Oleson, K. W., Swenson, S. C., Bonan, G., et al. (2019). The Community Land Model Version 5: Description of New Features, Benchmarking, and Impact of Forcing Uncertainty. *Journal of Advances in Modeling Earth Systems*, *11*(12), 4245–4287. https://doi.org/10.1029/2018MS001583

Li, F, Levis, S., & Ward, D. S. (2013). Quantifying the role of fire in the Earth system – Part 1: Improved global fire modeling in the Community Earth System Model (CESM1). *Biogeosciences*, *10*(4), 2293–2314. https://doi.org/10.5194/bg-10-2293-2013

Li, Fang, & Lawrence, D. M. (2017). Role of fire in the global land water budget during the twentieth century due to changing ecosystems. *Journal of Climate*, *30*(6), 1893–1908. https://doi.org/10.1175/JCLI-D-16-0460.1

Lombardozzi, D. L., Lu, Y., Lawrence, P. J., Lawrence, D. M., Swenson, S., Oleson, K. W., et al. (2020). Simulating Agriculture in the Community Land Model Version 5. *Journal of*

673 *Geophysical Research: Biogeosciences*, *125*(8), e2019JG005529.
674 https://doi.org/10.1029/2019JG005529
675 Long, M. C., Moore, J. K., Lindsay, K., Levy, M., Doney, S. C., Luo, J. Y., et al. (2021).
676 Simulations With the Marine Biogeochemistry Library (MARBL). *Journal of Advances in*
677 *Modeling Earth Systems*, *13*(12), e2021MS002647. https://doi.org/10.1029/2021MS002647
678 MacDougall, A. H., Frölicher, T. L., Jones, C. D., Rogelj, J., DamonMatthews, H., Zickfeld, K.,
679 et al. (2020). Is there warming in the pipeline? A multi-model analysis of the Zero
680 Emissions Commitment from CO_2. *Biogeosciences*, *17*(11), 2987–3016.
681 https://doi.org/10.5194/bg-17-2987-2020
682 Mathesius, S., Hofmann M., Caldeira K., & Schellnhuber H. J. (2015). Long-term response of
683 oceans to CO_2 removal from the atmosphere. *Nature Climate Change*, *5*, 1107–1113.
684 https://doi.org/10.1038/NCLIMATE2729
685 Matthews, D. H., Tokarska, K. B., Rogelj, J., Smith, C. J., MacDougall, A. H., Haustein, K., et al.
686 (2021). An integrated approach to quantifying uncertainties in the remaining carbon budget.
687 *Communications Earth & Environment*, *2*(1), 1–11. https://doi.org/10.1038/s43247-020-
688 00064-9
689 Matthews, H., Gillett, N., Stott, P., & Zickfeld, K. (2009). The proportionality of global warming
690 to cumulative carbon emissions. *Nature*, *459*(7248), 829–832.
691 https://doi.org/10.1038/nature08047
692 Melnikova, I., Boucher, O., Cadule, P., Ciais, P., Gasser, T., Quilcaille, Y., et al. (2021). Carbon
693 Cycle Response to Temperature Overshoot Beyond 2°C: An Analysis of CMIP6 Models.
694 *Earth's Future*, *9*(5), e2020EF001967. https://doi.org/10.1029/2020EF001967
695 O'Neill, B. C., Tebaldi, C., van Vuuren, D. P., Eyring, V., Friedlingstein, P., Hurtt, G., et al.
696 (2016). The Scenario Model Intercomparison Project (ScenarioMIP) for CMIP6. *Geosci.*
697 *Model Dev.*, *9*(9), 3461–3482. https://doi.org/10.5194/gmd-9-3461-2016

698 Oleson, K. W., Lawrence, D. M., Bonan, G. B., Drewniak, B., Huang, M., Charles, D., et al.
699 (2013). Technical Description of Version 4.5 of the Community Land Model (CLM). *NCAR*
700 *Technical Note*.
701 Orchard, V. A., & Cook, F. J. (1983). Relationship between soil respiration and soil moisture.
702 *Soil Biology and Biochemistry*, *15*(4), 447–453. https://doi.org/10.1016/0038-
703 0717(83)90010-X
704 Orr, J. C., Kwiatkowski, L., & Pörtner, H. O. (2022). Arctic Ocean annual high in pCO_2 could
705 shift from winter to summer. *Nature*, *610*(7930), 94–100. https://doi.org/10.1038/s41586-
706 022-05205-y
707 Park, S. W., & Kug, J. S. (2022). A decline in atmospheric CO_2 levels under negative emissions
708 may enhance carbon retention in the terrestrial biosphere. *Communications Earth and*
709 *Environment*, *3*(1), 2–9. https://doi.org/10.1038/s43247-022-00621-4
710 Rogelj, J., D. Shindell, K. Jiang, S. Fifita, P. Forster, V. Ginzburg, C. Handa, H. Kheshgi, S.
711 Kobayashi, E. Kriegler, L. Mundaca, R. Séférian, and M.V. Vilariño, 2018: Mitigation
712 Pathways Compatible with 1.5°C in the Context of Sustainable Development. In: *Global*
713 *Warming of 1.5°C. An IPCC Special Report on the impacts of global warming of 1.5°C*
714 *above pre-industrial levels and related global greenhouse gas emission pathways, in the*
715 *context of strengthening the global response to the threat of climate change, sustainable*
716 *development, and efforts to eradicate poverty* [Masson-Delmotte, V., P. Zhai, H.-O. Pörtner,
717 D. Roberts, J. Skea, P.R. Shukla, A. Pirani, W. Moufouma-Okia, C. Péan, R. Pidcock, S.
718 Connors, J.B.R. Matthews, Y. Chen, X. Zhou, M.I. Gomis, E. Lonnoy, T. Maycock, M.
719 Tignor, and T. Waterfield (eds.)]. Cambridge University Press, Cambridge, UK and New
720 York, NY, USA, pp. 93-174, https://doi.org/10.1017/9781009157940.004.
721 Sabine, C. L., Feely, R. A., Gruber, N., Key, R. M., Lee, K., Bullister, J. L., et al. (2004). The
722 Oceanic Sink for Anthropogenic CO_2. *Science, 305*(5682), 367–371.
723 https://doi.org/10.1126/science.1097403

Schlesinger, W. H., & Andrews, J. A. (2000). Soil respiration and the global carbon cycle. *Biogeochemistry*, *48*(1), 7–20. https://doi.org/10.1023/A:1006247623877

Schuur, E. A. G., McGuire, A. D., Schädel, C., Grosse, G., Harden, J. W., Hayes, D. J., et al. (2015). Climate change and the permafrost carbon feedback. *Nature*, *520*(7546), 171–179. https://doi.org/10.1038/nature14338

Schwinger, J. & Tjiputra, J. (2018). Ocean Carbon Cycle Feedbacks Under Negative Emissions. *Geophysical Research Letters*, *45*(10), 5062–5070. https://doi.org/10.1029/2018GL077790

Schwinger, J., Asaadi, A., Steinert, N. J., & Lee, H. (2022a). Emit now, mitigate later? Earth system reversibility under overshoots of different magnitude and duration. *Earth System Dynamics, 13*, 1641–1665. https://doi.org/10.5194/esd-13-1641-2022

Schwinger, J., Asaadi, A., Goris, N., & Lee, H. (2022b). Possibility for strong northern hemisphere high-latitude cooling under negative emissions. *Nature Communications*, *13*(1), 1095. https://doi.org/10.1038/s41467-022-28573-5

Smith, R., Jones, P., Briegleb, B., Bryan, F., Danabasoglu, G., Dennis, J., et al. (2010). *The parallel ocean program (POP) reference manual ocean component of the community climate system model (CCSM) and community earth system model (CESM). LAUR-01853* (pp. 1–140).

Takahashi, T., Olafsson, J., Goddard, J. G., Chipman, D. W., & Sutherland, S. C. (1993). Seasonal variation of CO_2 and nutrients in the high-latitude oceans: A comparative study. *Global Biogeochemical Cycles*, *7*(4), 843–878. https://doi.org/10.1029/93GB02263

Takahashi, Taro, Sutherland, S. C., Wanninkhof, R., Sweeney, C., Feely, R. A., Chipman, D. W., et al. (2009). Climatological mean and decadal change in surface ocean pCO_2, and net sea-air CO_2 flux over the global oceans. *Deep-Sea Research Part II: Topical Studies in Oceanography*, *56*(8–10), 554–577. https://doi.org/10.1016/j.dsr2.2008.12.009

Thompson, M. V, Randerson, J. T., Malmström, C. M., & Field, C. B. (1996). Change in net primary production and heterotrophic respiration: How much is necessary to sustain the

terrestrial carbon sink? *Global Biogeochemical Cycles*, *10*(4), 711–726. https://doi.org/https://doi.org/10.1029/96GB01667

United Nations Framework on Climate Change (UNFCCC) (2015). Adoption of the Paris Agreement, 21st Conference of the Parties. Available at: http://unfccc.int/resource/docs/2015/cop21/eng/l09r01.pdf.

Wang, J., Sun, J., Xia, J., He, N., Li, M., & Niu, S. (2018). Soil and vegetation carbon turnover times from tropical to boreal forests. *Functional Ecology*, *32*(1), 71–82. https://doi.org/10.1111/1365-2435.12914

Wetzel, P., Winguth, A., & Maier-Reimer, E. (2005). Sea-to-air CO2 flux from 1948 to 2003: A model study. *Global Biogeochemical Cycles*, *19*, 1–19. https://doi.org/10.1029/2004GB002339

Wigley, T. M. L. (2005). The Climate Change Commitment. *Science*, *307*(5716), 1766–1769. https://doi.org/10.1126/science.1103934

Wu, P., Wood, R., Ridley, J., & Lowe, J. (2010). Temporary acceleration of the hydrological cycle in response to a CO_2 rampdown. *Geophysical Research Letters, 37,* L12705. https://doi.org/10.1029/2010GL043730

Xu, L., Myneni, R. B., Chapin III, F. S., Callaghan, T. V, Pinzon, J. E., Tucker, C. J., et al. (2013). Temperature and vegetation seasonality diminishment over northern lands. *Nature Climate Change*, *3*(6), 581–586. https://doi.org/10.1038/nclimate1836

Zhu, Z., Piao, S., Myneni, R. B., Huang, M., Zeng, Z., Canadell, J. G., et al. (2016). Greening of the Earth and its drivers. *Nature Climate Change*, *6*(8), 791–795. https://doi.org/10.1038/nclimate3004

Zickfeld, K., MacDougall, A. H., & Damon Matthews, H. (2016). On the proportionality between global temperature change and cumulative CO_2 emissions during periods of net negative CO_2 emissions. *Environmental Research Letters*, *11*(5), 055006. https://doi.org/10.1088/1748-9326/11/5/055006

776 Ziehn, T., Lenton, A., & Law, R. (2020). An assessment of land-based climate and carbon
777 reversibility in the Australian Community Climate and Earth System Simulator. *Mitigation*
778 *and Adaptation Strategies for Global Change*, *25*(4), 713–731.
779 https://doi.org/10.1007/s11027-019-09905-1
780

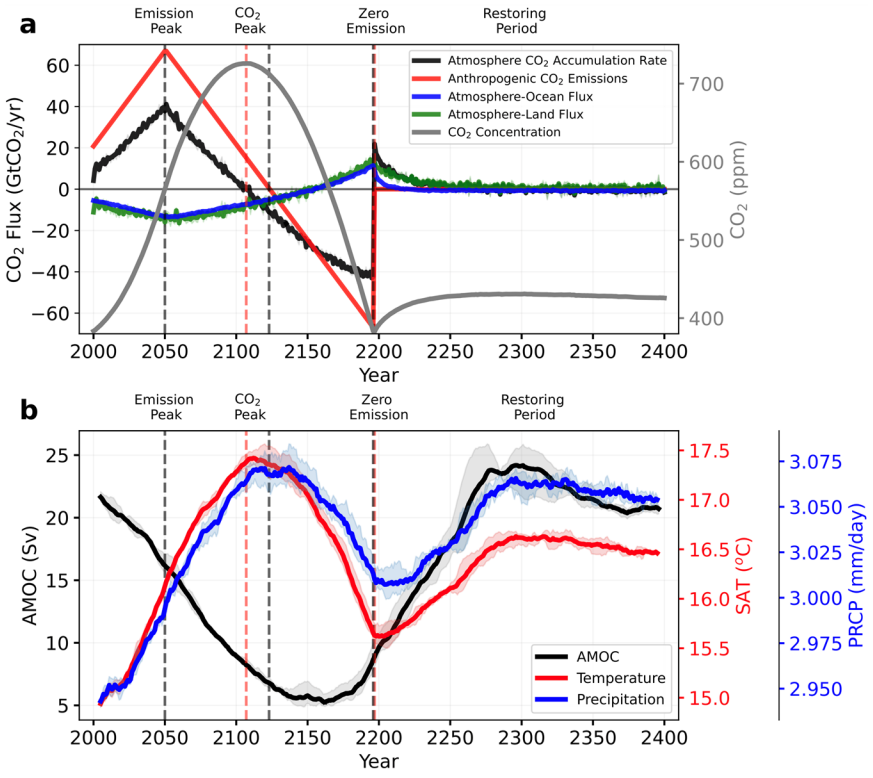

781

782 **Figure 1.** Global mean responses of surface CO_2 fluxes and the climate system in an
783 idealized negative emissions scenario. (a) Time-series of atmospheric CO_2 accumulation
784 rate, anthropogenic CO_2 emissions, land–atmosphere and ocean–atmosphere CO_2 fluxes
785 (positive: surface to the atmosphere), and atmospheric CO_2 concentrations. (b) Time-series
786 of the 11-year running means of global annual mean surface air temperature (SAT) and
787 precipitation (PRCP) and the strength of the Atlantic Meridional Overturning Circulation
788 (AMOC). The AMOC strength is defined as the average of the annual mean Atlantic
789 meridional ocean stream function from 35° to 45° N at a depth of 1,000 m. The solid lines
790 and shaded areas respectively show the ensemble mean and the range of 95% confidence
791 interval, based on the bootstrap method. The peak of anthropogenic emissions and the onset
792 of negative and zero emissions (restoring period) are indicated by the grey dashed vertical
793 line. The points of maximum and minimum CO_2 levels are indicated by the red dashed
794 vertical line.

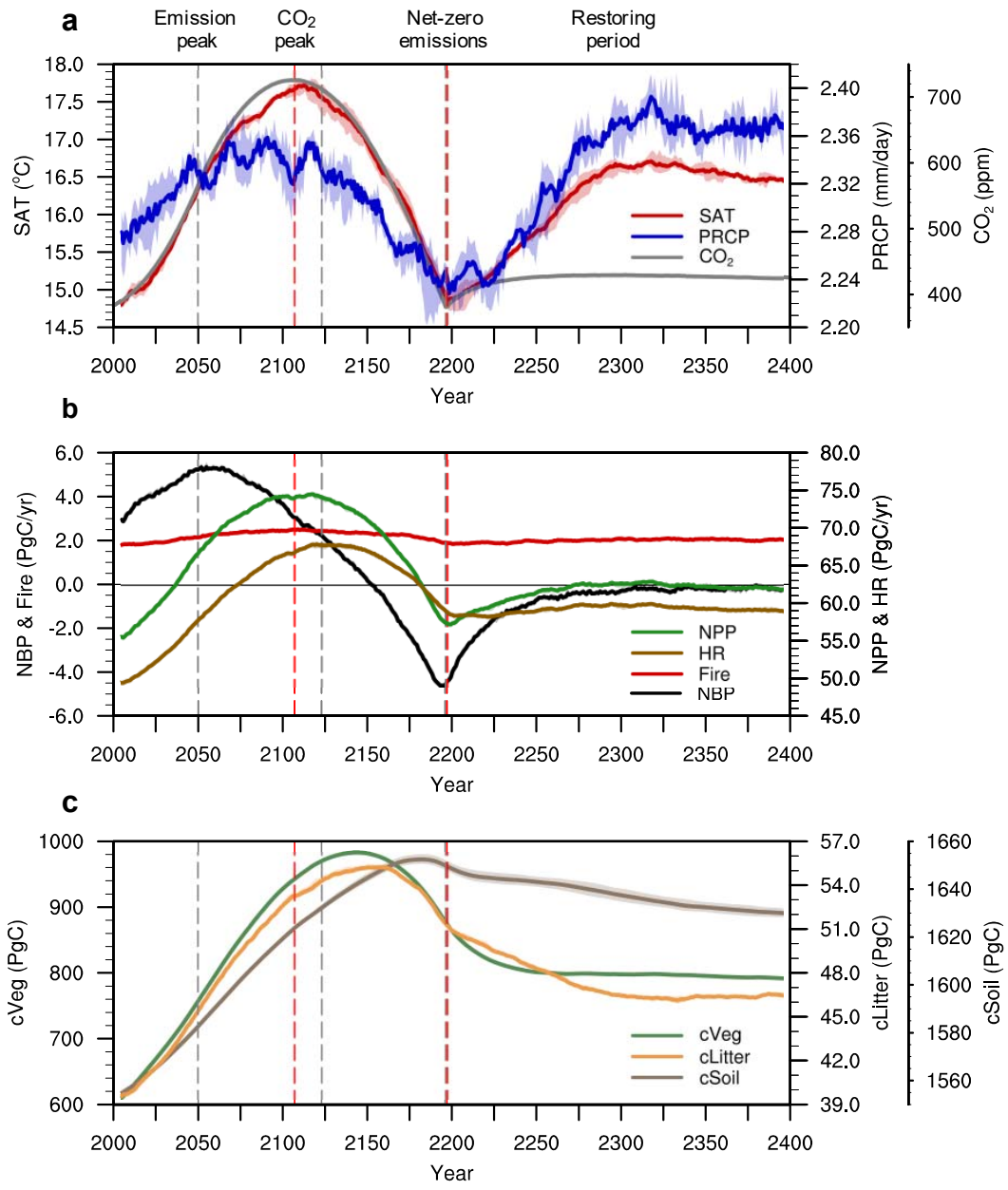

795

796 **Figure 2.** Temporal evolution of global terrestrial carbon fluxes and stocks. (a) Time-series
797 of the annual mean land SAT and PRCP and the atmospheric CO_2 concentration; (b) annual
798 net primary production (NPP), heterotrophic respiration (HR), fire C loss (Fire), and net
799 biome productivity (NBP); (c) annual mean vegetation, litter, and soil C stocks. All values
800 except for the CO_2 concentrations are smoothed by the 11-year moving average. Solid lines
801 and shaded areas respectively show the ensemble mean and the range of 95% confidence
802 interval, based on the bootstrap method.

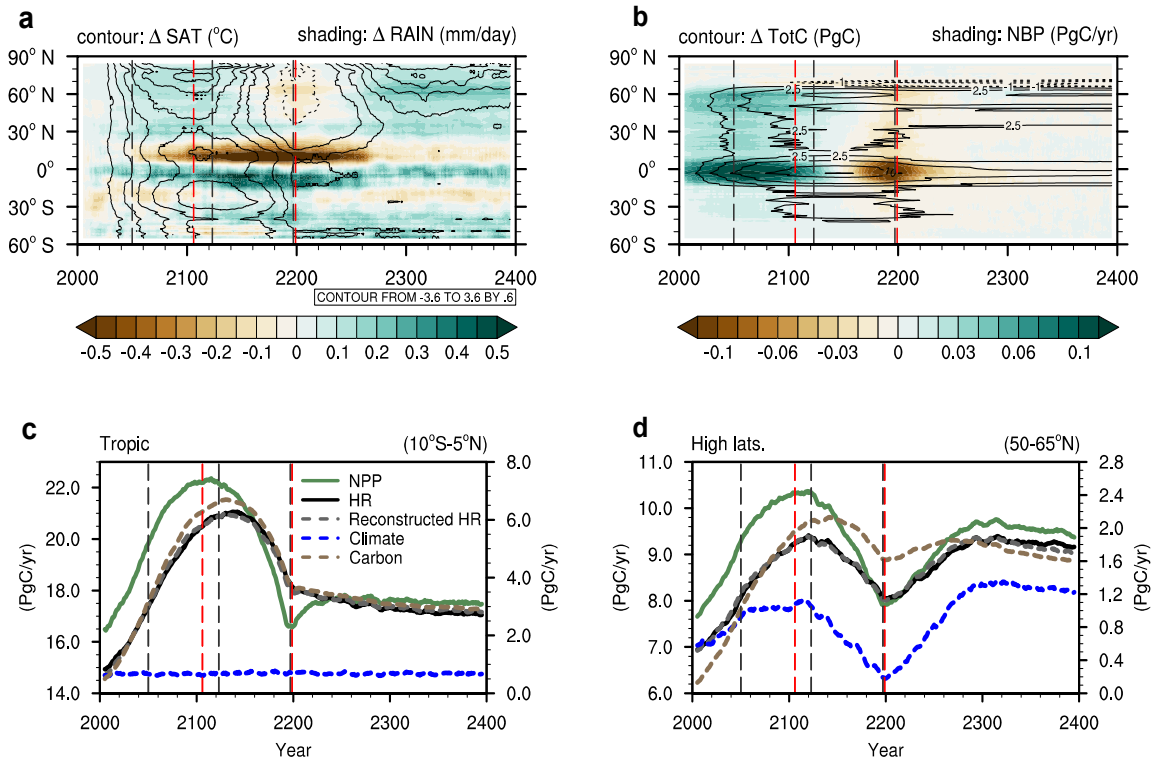

803

804 **Figure 3.** Latitudinal differences in the evolution of the climate system and the terrestrial
805 carbon cycle. (a) Time-latitude diagrams of the annual mean anomalies of land SAT
806 (contour) and PRCP (shading) relative to the year 2000; (b) annual mean total terrestrial C
807 stock anomaly (contour) relative to the year 2000 and annual NBP (shading). All values
808 are the ensemble means and smoothed by the 11-year moving average. (c) Time-series of
809 the annual NPP and HR and the reconstructed HR from a multiple linear regression based
810 on climate factors (normalized SAT and PRCP) and factors associated with the terrestrial
811 C cycle (normalized NPP, litter C, and soil C) in the tropics and (d) the mid-high latitudes
812 (left axis: NPP, HR, and reconstructed HR; right axis: contributions of each factor to the
813 change of HR). All calculations were performed after taking the 11-year running mean and
814 all values are the ensemble mean.

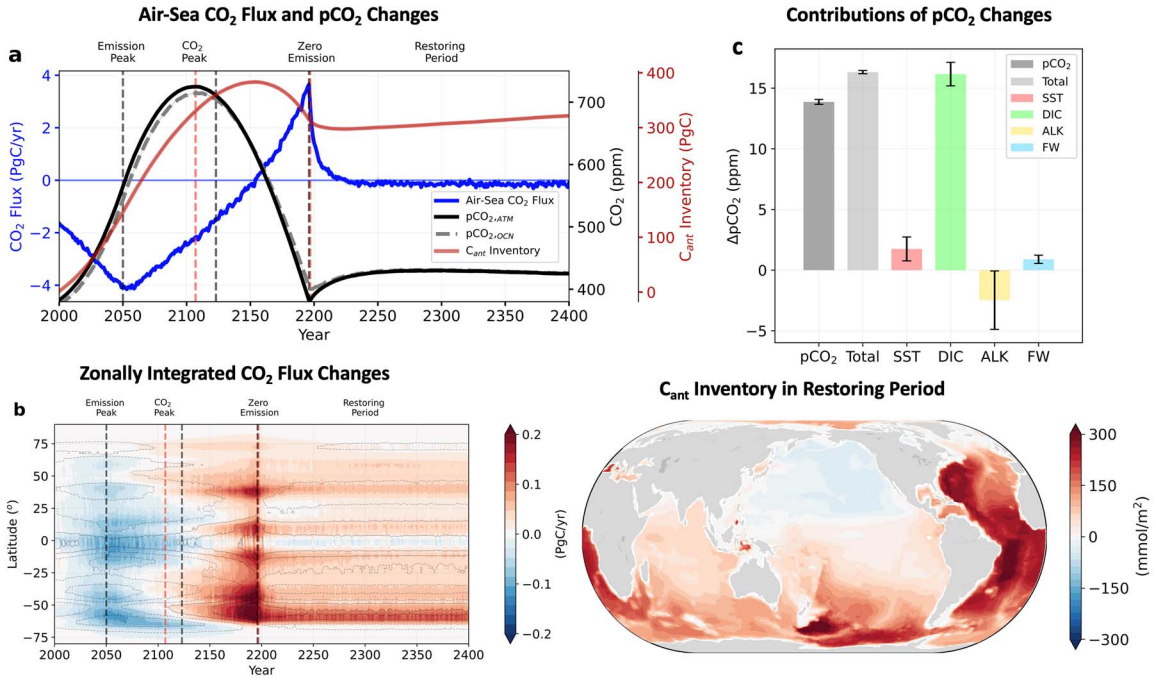

Figure 4. Temporal evolution of global ocean carbon systems. (a) Time-series of the annual mean air-sea CO_2 flux (blue), cumulative ocean CO_2 uptake (red), partial pressure of CO_2 (pCO_2) in atmosphere (black) and ocean (grey). The solid lines and shadings respectively show the ensemble mean and the range of 95% confidence level based on the bootstrap method. (b) Time-latitude diagrams of annual mean changes in air-sea CO_2 flux anomaly. Selected black isolines represent the air-sea CO_2 flux from -0.2 to 0.2 PgC/yr with 0.1PgC/yr difference levels. Dashed and solid lines mean negative and positive air-sea CO_2 flux, respectively. Negative flux represents a carbon sink into the ocean. (c) Contributions of changes in the ocean pCO_2 for each component; sea surface temperature (SST), dissolved inorganic carbon (DIC), total alkalinity (ALK), and freshwater (FW). (d) C_{ant} inventory changes in the restoring period.